Smart Structures and Systems, *Vol. 32, No. 6 (2023) 371-382*
https://doi.org/10.12989/sss.2023.32.6.371

Load rating of box girder bridges based on rapid testing using moving loads

Hong Zhou [a], Dong-Hui Yang*, Ting-Hua Yi [b] and Hong-Nan Li [c]

School of Civil Engineering, Dalian University of Technology, Dalian 116023, China

(*Received February 20, 2023, Revised October 22, 2023, Accepted November 16, 2023*)

Abstract. Box girder bridges are now widely used in bridge construction, and it is necessary to perform load rating regularly to evaluate the load capacity of box girder bridges. Load testing is a common measure for load rating. However, the bridge must be loaded by many trucks under different loading conditions, which is time-consuming and laborious. To solve this problem, this paper proposes a load rating method for box girder bridges based on rapid moving loads testing. The method includes three steps. First, the quasi-influence factors of the bridge are obtained by crossing the bridge with rapidly moving loads, and the structural modal parameters are simultaneously obtained from the dynamic data to supplement. Second, an objective function is constructed, consisting of the quasi-influence factors at several measurement points and structural modal parameters. The finite element model for load rating is then updated based on the Rosenbrock method. Third, on this basis, a load rating method is proposed using the updated model. The load rating method proposed in this paper can considerably reduce the time duration of traditional static load testing and effectively utilize the dynamic and static properties of box girder bridges to obtain an accurate finite element model. The load capacity obtained based on the updated model can avoid the inconsistency of the evaluation results for the different structural members using the adjustment factors specified in codes.

Keywords: box girder bridge; load rating; model updating; objective function; rapid load testing

1. Introduction

Box girder bridges constitute a large proportion of the existing bridges due to their driving comfort, high stiffness, and good load capacity. With increasing operation life, the load capacity of box girder bridges is decreasing due to material deterioration and other adverse factors (Yang *et al*. 2017, 2018). Once an accident occurs, it will seriously impede traffic, resulting in economic losses and casualties. Therefore, to ensure the safe operation of bridges, load capacity evaluation of bridges is an essential part of bridge maintenance and management procedures (Sun *et al*. 2021).

Load capacity is one of the most significant performance aspects of box girder bridges, which typically serve as vital transportation links. Many countries have issued codes providing recommendations for a standardized bridge load capacity evaluation procedure (AASHTO 2011, MOT 2011). Bridge load rating provides a basis for determining the safe load capacity of a bridge. It usually combines inspection, material testing, load testing, and analysis calculations according to the US code *The manual for bridge evaluation* (*MBE*) (AASHTO 2011). Field load testing is a critical part of bridge load rating because it directly reflects the current performance of the bridge through loading (Abedin *et al*. 2022). However, load testing typically requires multiple trucks and complex loading procedures, which are time-consuming and costly. In addition, traffic disruptions are necessary for an extended period to implement load testing. In the current code-based evaluation methods for bridge capacity, preliminary rating factors are determined by calculating the load effects and structure resistance of the bridge. Since both the calculation of load effects and structure resistance are based on simplified mechanical models, the results of load testing are applied to adjust the rating factors and determine the final load rating results (Schlune *et al*. 2009).

Because the load testing is time-consuming and laborious, how to use the rapid testing to replace the traditional load testing and carry out the load rating becomes an urgent problem. Currently, some scholars are attempting to simplify the load testing scheme by using a light load testing method with fewer load vehicles crossing the bridge to evaluate its load capacity. Zheng *et al*. (2022) proposed obtaining the structural influence line as a proxy model of the actual bridge structure for load capacity evaluation using only a small number of load vehicles. However, the influence lines obtained reflect only the structural stiffness information and cannot provide the necessary physical parameters, such as material properties and section configuration, for evaluating load capacity degradation. To address the issue of proxy models, such as influence lines, not providing sufficient information about bridge structures, the model updating technique is utilized by many researchers to obtain an accurate model that matches the real bridge. Sanayei *et al*. (2012) conducted a static truck load testing on a continuous girder bridge and updated the finite element model of this bridge based on the

*Corresponding author, Ph.D., Associate Professor,
E-mail: dhyang@dlut.edu.cn
[a] Ph.D. Student, E-mail: 22006082@mail.dlut.edu.cn
[b] Professor, E-mail: yth@dlut.edu.cn
[c] Professor, E-mail: hnli@dlut.edu.cn

ISSN: 1738-1584 (Print), 1738-1991 (Online)

strain data obtained. Altunişik *et al*. (2020) completed the frequency extraction of a historical timber bridge based on environmental vibrations and model updating based on the frequency results. Xin *et al*. (2022) updated the finite element model of a highway bridge using strain data obtained from bridge static load testing and modal information identified from measured bridge acceleration responses under operational traffic conditions. By simultaneously utilizing both static and dynamic data for updating bridge models, a finite element model that better matches the actual structure can be obtained.

The static and dynamic response of the bridge need to be obtained from rapid testing to update the initial finite element model of the bridge. Static loads are generally provided by trucks. The bridge response can be approximated as static when the truck travels slowly across the bridge, which can be used to obtain the influence line (Yang *et al*. 2022). Martini *et al*. (2022) completed the model updating of a laboratory bridge model using displacement influence lines. The influence line, as a simplified method, provides the possibility of using moving loads for rapid testing and model updating. Dynamic characteristics can be quickly and easily extracted in various ways and can even be obtained based on the dynamic response during operation. Therefore, a rapid testing procedure for bridge evaluation can be proposed.

This paper proposes a method for load rating of box girder bridges based on rapid testing using a moving load. First, the static and dynamic characteristics of box girder bridges are acquired, which are defined as the quasi-influence factors obtained by crossing the bridge with a moving load and the dynamic data obtained from the dynamic testing. Then, an objective function is constructed, consisting of the quasi-influence factors at multiple spatial measurement points and structural modal parameters. A model updating procedure suitable for box girder bridges is proposed. In addition, a load rating method based on the updated model is proposed. Finally, a field application was conducted on a box girder bridge to complete the load rating evaluation process using the above evaluation method.

2. Rapid static and dynamic testing of a box girder bridge

Load testing is typically conducted to evaluate changes in the performance of bridges. The responses of the bridge can be analyzed to determine if deterioration has occurred. However, traditional load testing methods need improvement due to their high time and labor costs. This paper proposes a method for rapidly load testing bridges using moving loads. By moving the load on the bridge deck, a time-history response curve reflecting the overall performance of the bridge can be obtained, which can be considered as the quasi-influence factors of the bridge. These quasi-influence factors significantly increase the response information spatially and can effectively reduce the number of required measurement points. In addition, structural modal parameters are obtained through dynamic testing provide valuable supplementary information to the static data. Finally, the static and dynamic parameters are applied as the basis for evaluating the bridge's load capacity.

2.1 Acquisition of quasi-influence factor using moving loads

According to Betti's law (Timoshenko and Young 1968), the deflection influence line at a location on a bridge is numerically equal to the deformation curve when a unit-concentrated load is applied to that location. The law also applies to other responses. Similarly to the influence line, the quasi-influence factor can be defined as the response obtained by a multi-axial load traveling on a bridge, rather than a unit-concentrated load. Therefore, the quasi-influence factors obtained from the moving load reflect the performance condition of the bridge over its entire span. These quasi-influence factors are obtained by measuring the time-history response at only a few locations, effectively reducing the number of required sensors. These quasi-influence factors can be obtained at low cost by renting only a loading truck and installing a small number of sensors. The loading process should ensure the following principles:

1. The vehicle should cross the bridge at a crawl speed of approximately 5km/h to minimize dynamic effects (Sanayei *et al*. 2012).
2. The vehicle should travel in a straight line across the bridge within a single lane without changing lanes.
3. Depending on the number of lanes designed for the bridge, the vehicle must travel at least once in each lane.

These principles ensure that the vehicle covers most of the bridge, which can reflect the performance variation of the whole bridge. The load testing scheme is shown in Fig. 1.

For quasi-influence factor measurements, the commonly measured responses are strain and deflection. The measurement location is typically chosen at the location with the maximum structural responses, usually the mid-span section, to ensure clear and accurate measurement of the quasi-influence factors. For deflection measurement, the distribution of deflection is basically the same throughout the cross-section, so only one to two measurement points need to be arranged at the bottom of the girder to obtain the deflection variation at one cross-section. However, for strain measurement, the strain distribution on the box girder

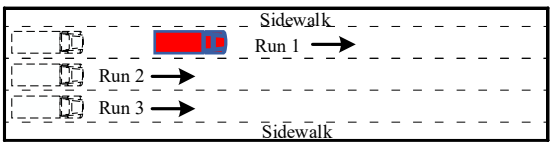

(a) Testing scheme

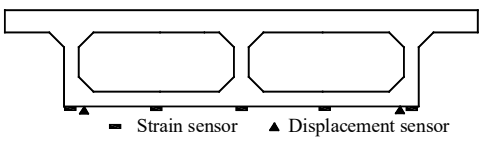

(b) Sensor arrangement

Fig. 1 Moving load testing

cross-section is variable due to the shear lag effect. Therefore, multiple strain sensors should be arranged at the same section to avoid misunderstanding the strain distribution due to limited strain measurement points. To avoid interference with vehicle load testing, strain sensors are generally arranged on the bottom or side of the box girder. The bottom of the box beam is an ideal position for strain transducers because the largest vehicle-induced strain usually occurs at this position. In addition, to capture the uneven distributed strain due to the shear lag effects in box girder sections, the strain sensors should be evenly arranged at the bottom of the box girder. A typical strain senor arrangement for a single-box two-cell box girder is shown in Fig. 1(b).

2.2 Structural characteristic extraction based on dynamic testing

The dynamic characteristics of bridges are directly related to the mass and stiffness matrix of the bridge. Therefore, the dynamic characteristics, which are the modal parameters, can also be applied in load capacity evaluation of bridges. Modal parameters of bridges are identified by subjecting the bridge to forced or free vibrations. The modal parameters of bridges can be identified by measuring only the structural vibration under ambient excitation. The excitation can usually be unknown random environmental excitation, such as wind or vehicle impact, or known artificial excitation, such as impulse load or simple harmonic excitation. Modal parameter identification methods are usually divided into time domain methods and frequency domain methods. Frequency domain methods include peak picking (Ren and Zong 2004), frequency domain decomposition (Brincker *et al*. 2001) and so on. The problem of frequency domain methods is the large error of frequency spectral. Because of the fence effect and spectral leakage, the modal parameter identification results are not so ideal. Meanwhile, time-domain methods perform better in this aspect. The stochastic subspace technique (Xue *et al*. 2022) is chosen due to being a mature method in the time domain method of modal parameter identification. Stabilization diagram is used in stochastic subspace technique to remove spurious modes, which makes the identified modal parameters more reliable.

3. Finite element model for load rating of box girder bridges

3.1 Modeling method for box girder bridge

The common finite element models for simulating bridges are the beam element model, shell element model and solid element model, as shown in Fig. 2. In the beam element model, the entire bridge is simplified as a single beam or multiple beams. In the shell element model, each member of the bridge is considered a plate, which is more suitable for the simulation of bridges with more plate members. In the solid model, the bridge is simulated exactly according to the shapes and materials of the members, so the results are the most accurate, but the calculation and

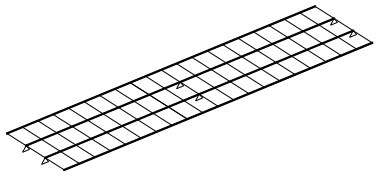

(a) Beam element model

(b) Shell element model

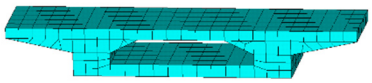

(c) Solid element model

Fig. 2 Finite element models for a box girder bridge

analysis time is longer. The internal forces and deformations are not uniformly distributed in the cross-section of box girder bridges due to the torsional and shear lag effect. To simulate the force characteristics of a box girder bridge in detail, it is unrealistic to reduce the whole bridge to a single beam. The shell element model and solid model can simulate the box girder cross-section and provide accurate analysis results, so these models can reflect the performance of box girder bridges more successfully (Zhang *et al*. 2010). The solid model is generally considered to be the most accurate model for simulating structural performance. However, it is not recommended for iterative calculations due to the large number of nodes and extended computation time. Therefore, considering computation time and accuracy, the shell element model is the better model form for simulating box girder bridges.

3.2 Combined static and dynamic objective functions

The initial finite element model typically deviates from the actual bridge behavior due to differences in modeling and actual structural parameters. Model updating is applied to minimize these discrepancies. To effectively reflect the difference between the model response and the actual structural response, a suitable objective function needs to be established to quantify the error and transform the model updating problem into a mathematical problem, as in Eq. (1).

$$\min(F(\theta)) \quad \text{s.t. } \theta_1 \le \theta \le \theta_2 \tag{1}$$

where $F(\theta)$ is the objective function; θ is the updating parameter; and θ_1 and θ_2 are the lower and upper boundaries of the updating parameter, respectively.

3.2.1 Objective function of spatial strain quasi-influence factor

In practical validation, the strain results of the model still do not exactly match the measured strain distribution. This is due to the fact that the model established by shell

element is homogeneous. However, in reality, the box girder bridge is composed of reinforcing steel and concrete, in which the prestressing steel reinforcement will have a large influence on the stiffness distribution of the cross-section. As a result, the shear lag and torsion effects are affected by the above, and the model established by shell element will have some errors in the strain with the actual bridge. In the final load rating, the internal forces of the critical section of the box girder are used. Therefore, in this condition, even if local stresses are inaccurate, the overall internal forces can be guaranteed to be consistent. The bottom plate of the box girder is the main location for strain measurement. The axial force T of the bottom plate can be obtained from the following equation

$$T(y_j) = E \cdot t \cdot \int \varepsilon(x, y_j) dx \tag{2}$$

where E is the material elastic modulus of the bottom plate; t is the thickness of the bottom plate; x is the coordinate of the strain measuring point along the transverse bridge direction; y_j is the coordinate of the test vehicle along longitudinal bridge direction when the jth strain sample is measured; and $\varepsilon(\cdot)$ is the strain distribution function. Once the strain in the bottom plate is known, the axial force in the bottom plate can be calculated. The strain distribution on the bottom plate is in the form of a cubic function (Chang 2004). Therefore, the strain distribution function of the entire bottom plate can be fitted with a small number of strain measurement points to calculate the axial force in the bottom plate. The strain objective function F_1 can be constructed as Eq. (3)

$$F_1 = \frac{1}{mn} \sum_{i=1}^{m} \sum_{j=1}^{n} \alpha_i \left(\frac{T_i^e(y_j) - T_i^a(y_j)}{T_i^e(y_j)} \right)^2 \tag{3}$$

where m is the number of bridge crossing by the testing vehicle; n is the total sampling number of strain during a test vehicle crossing the bridge and α is the weight coefficient. T_i^e and T_i^a represent the measured value and the theoretical calculated value, respectively.

3.2.2 Objective functions of frequency and mode shapes

As a complement to the static response, dynamic characteristics are further used to update the model for box girder bridges. These dynamic characteristics include frequency and mode shape. The objective function for the structural frequency is established based on the residuals of each order frequency, and the objective function for the mode shape is determined using the modal assurance criterion (MAC). The objective functions F_2 and F_3 for the structural frequency and mode shape can be shown as follows (Jung and Kim 2013)

$$F_2 = \frac{1}{k} \sum_{i=1}^{k} \beta_i \left(\frac{f_i^e - f_i^a}{f_i^e} \right)^2 \tag{4}$$

$$MAC_i = \frac{(\boldsymbol{\Phi}_i{}^{eT} \boldsymbol{\Phi}_i{}^a)^2}{(\boldsymbol{\Phi}_i{}^{aT} \boldsymbol{\Phi}_i{}^a)(\boldsymbol{\Phi}_i{}^{eT} \boldsymbol{\Phi}_i{}^e)} \tag{5}$$

$$F_3 = \frac{1}{k} \sum_{i=1}^{k} \gamma_i \sqrt{\frac{1 - MAC_i}{MAC_i}} \tag{6}$$

where k is the number of modal orders involved in the model updating; $f_i{}^e$ and $f_i{}^a$ are the measured and theoretical values of the ith order frequency, respectively; $\boldsymbol{\Phi}_i{}^e$ and $\boldsymbol{\Phi}_i{}^a$ are the measured and theoretical values of the ith order mode shape vector, respectively; and β and γ are weight coefficients, which is usually taken as 1.

3.2.3 Normalized combination of objective functions

The static and dynamic objective functions mentioned above need to be combined into a single objective function for model updating. Considering the different importance and order of magnitude of different response objective functions, weighting coefficients need to be used in the combination. Therefore, these objective functions can be summed with suitable weighting factors, as shown in Eq. (7).

$$F(\theta) = \sum \lambda_i F_i(\theta) \tag{7}$$

where λ is the weighting coefficient when combining objective functions. Typically, each objective function should be equally weighted. However, in practice, when the initial value of an objective function is too low, it is found to be easy to cause insufficient updating of structural parameters related to this objective function. Therefore, the weighting coefficients are modified in combination. The inverse of the initial value of each objective function is used as the weighting coefficient, and then each objective function is normalized. The formula of the combined objective function is as follows

$$\lambda_i = \frac{1}{F_{i,0}} \tag{8}$$

$$F = \sum_{i=1}^{nr} \frac{F_i}{F_{i,0}} \tag{9}$$

where $F_{i,0}$ is the initial value of F_i, and nr is the number of objective functions to be combined.

3.3 Load rating model updating

Parameters to be optimized for updating the bridge model should be determined based on the following two principles: first, the parameters are prone to change in practice, resulting in inconsistency with the model; second, optimization parameters need to be sufficiently sensitive to the objective function. The commonly used method of selecting optimization parameters relies on engineering experience or sensitivity analysis (Lin *et al*. 2022). It is recommended to select alternative optimization parameters

based on engineering experience first and then use sensitivity analysis to filter out the more sensitive parameters. These parameters are used as optimization parameters for the model updating. The sensitivity analysis equation is as follows

$$S_g = \frac{(F(\theta + \Delta\theta) - F(\theta))/F(\theta)}{\Delta\theta/\theta} \quad (10)$$

where $\Delta\theta$ is the small perturbation to the optimization parameters and can be set to 1%. The sensitivity can be determined by adding $\Delta\theta$ to the initial value of the optimization parameters and observing the change rate of the objective function.

However, certain optimization parameters, such as the additional stiffness of the support, often have a wide range of variation, resulting in a relatively small rate of change in the objective function. The sensitivity of these parameters cannot be compared to the sensitivity of other optimization parameters. Using Eq. (10) to calculate the sensitivity results in an extremely small value for these parameters. In fact, the additional stiffness contributes greatly to the objective function and structural performance (Hester *et al*. 2019). Therefore, for this type of parameter, Eq. (10) needs to be modified. The modified equation for the sensitivity analysis is as follows

$$S_g = (F(\theta_2) - F(\theta_1))/F(\theta_1) \quad (11)$$

where θ_1 and θ_2 are the lower and upper boundaries of the updating parameter, respectively.

After determining the objective function and optimization parameters, the problem of the model updating can be transformed into a mathematical optimization problem. An accurate finite element model can be obtained by selecting a suitable optimization algorithm to update the initial model. The principles of optimization algorithm selection should be fast convergence, low number of iterations and high optimization accuracy. In this paper, the Rosenbrock algorithm (an unconstrained optimization algorithm) is chosen. Compared with other unconstrained optimization algorithms, this algorithm has an extra step of "axis rotation" in the optimization process, which enhances the speed and approximation quality of the optimization (Zordan *et al*. 2014). Once the model updating is completed, the model can be used for load rating, which can better reflect the current performance of the bridge.

4. Load rating method and procedure

The United States completed most of its infrastructure construction in the last century. In order to ensure the safety of bridges in service, as early as 1930, the United States began to develop the relevant testing codes, so far it has been nearly a century of development and verification. Most countries have borrowed the US code for bridge load capacity evaluation. As a result, the US Code is chosen for load capacity evaluation. In the US code *MBE*, the evaluation result for load capacity is obtained by rating factor RF_T, which is calculated according to Eqs. (11) and (12).

$$RF_T = RF_c \cdot K = \frac{C - (\gamma_{DC})(DC) - (\gamma_{DW})(DW) \pm (\gamma_P)(P)}{(\gamma_{LL})(LL + IM)} \cdot K \quad (12)$$

where RF_c is the rating factor based on calculations prior to incorporation testing results; K is the adjustment factor; and C is the load capacity. For the strength limit state, $C = \varphi_c \varphi_s \varphi R_n$, where φ_c, φ_s, φ and R_n represent the condition factor, system factor, load and resistance factor design (LRFD) resistance factor, and nominal member resistance, respectively. DC is the dead load effect due to structural components and attachments; DW is the dead load effect due to wearing surfaces and utilities; P is the permanent loads other than dead loads; LL is the live load effect; IM is the dynamic load allowance; and γ is the corresponding coefficient for each load effect. These factors can be found in the code *MBE*. The adjustment factor K can be obtained as follows

$$K = 1 + K_a K_b \quad (13)$$

where K_a accounts for both the benefit derived from the load testing and consideration of the section factor, and K_b accounts for the understanding of the load testing results compared with the results predicted by theory.

Adjustment factors are added to account for the differences between the design model and the actual bridge. These adjustment factors are obtained through load testing to further modify the adjustment factor. However, the same adjustment factor is applied to decrease the differences between the design model and the actual bridge for the different structural components, and it cannot consider the performance variations among different parts of the bridge. Therefore, the method proposed in this paper can replace the adjustment factor and directly calculate the rating factor through the accurate updated finite element model. The rating factor RF can be shown as Eq. (14).

$$RF = \frac{C - (\gamma_{DC})(DC_m) - (\gamma_{DW})(DW_m) \pm (\gamma_P)(P_m)}{(\gamma_{LL})(LL_m + IM_m)} \quad (14)$$

where the subscript m represents the load effect obtained from the updated model.

The load effect in Eq. (12) is replaced by the load effect of the updated model, which is consistent with the load effect of an actual bridge. This approach allows for the direct evaluation of the current live load resistance in the bridge structure with respect to the live load effect, without the need to adjust the result using an adjustment factor.

Finally, the safe load capacity of the bridge can be determined according to the rating factor, as shown in Eq. (15)

$$RT = RF \times W \quad (15)$$

where RT is the rating in tons for trucks used in computing the live load effect and $W$is the weight in tons of trucks used in computing the live load effect. RT can be considered the quantification of load capacity.

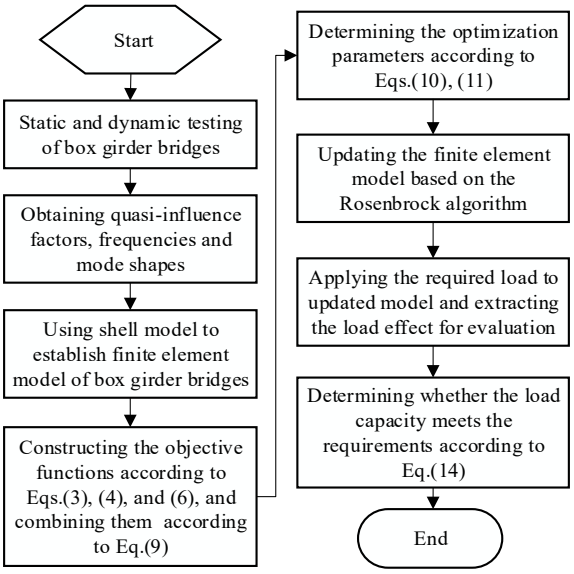

Fig. 3 Flow chart of load capacity evaluation of box girder bridge

The entire procedure of the rapid testing and load capacity evaluation of the box girder bridge is shown in Fig. 3. Based on the proposed procedure, a field application example is presented in the subsequent section.

5. Field application

5.1 Box girder bridge field testing

The test bridge is a prestressed concrete continuous beam bridge with the cross-section being a single-cell box and two spans of 24 m + 24 m = 48 m. The bridge width is 6 m, and the effective pedestrian width is 5.5 m. This bridge is a footbridge with the design pedestrian load of 5 kN/m^2. Concrete with a compressive strength of 32.4 MPa is applied in the superstructure and pier. The photograph and configurations of the test bridge are shown in Fig. 4. Three kinds of testing were conducted: the moving load testing, dynamic testing, and static load testing.

5.1.1 Rapid moving load testing

The moving load testing was conducted to obtain the strain variation of the bridge under the moving load. The test bridge is a footbridge that cannot be loaded by the testing trucks. Therefore, a moving trolley loaded with a water tank was used to load the bridge to obtain the strain quasi-influence factors of the bridge (Fig. 5). The total mass of the trolley and human was approximately 750 kg. The bridge was divided into three equal lanes, and the trolley was driven along each of these three lanes at a crawl speed to minimize the dynamic effect. It is worth mentioning that the moving trolley traveled back and forth on each path more than twice as a way to obtain reliable results. The driving scheme followed the method shown in Fig. 1. The trolley paused for approximately 10 s when it reached the

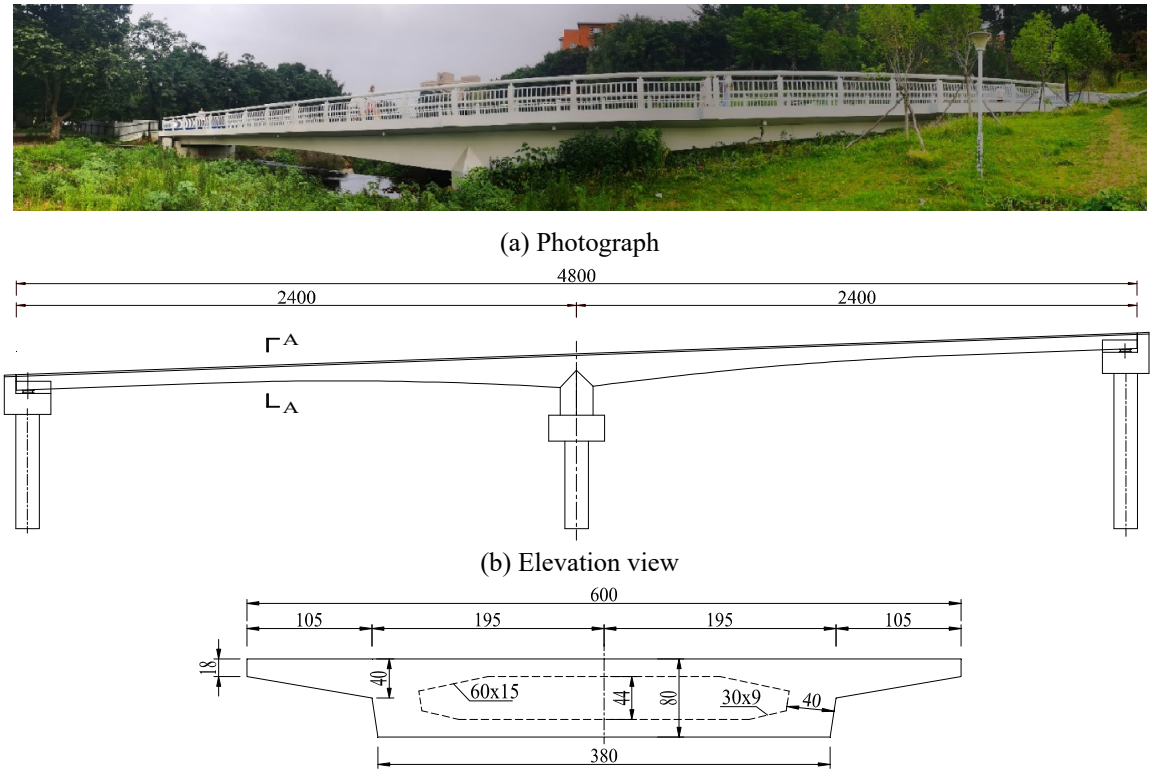

(a) Photograph

(b) Elevation view

(c) Cross Section A-A

Fig. 4 Photograph and configurations of the test bridge (unit: cm)

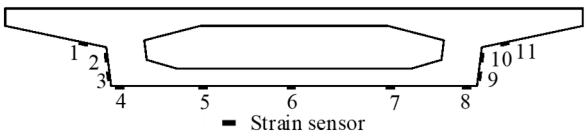

(a) Strain sensor arrangement in the middle of the left span

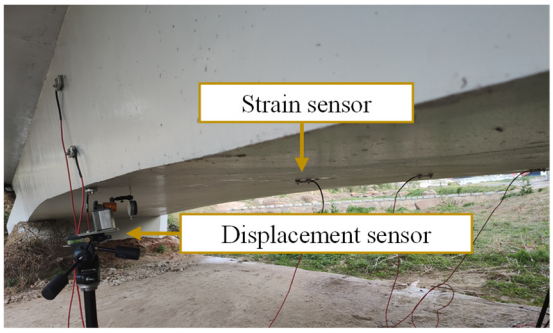

(b) Field installation of sensors

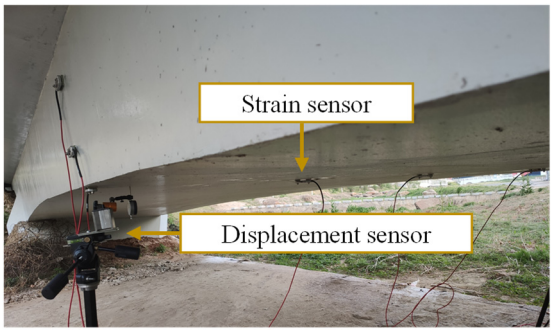

(c) Moving trolley for load

Fig. 5 Moving load testing

middle of each span to obtain a more stable maximum strain.

In general, strain sensors were installed in each span to obtain the maximum responses. The measurement equipment used in this paper is a wireless strain measurement system. The resolution of strain sensor is 0.1 με. Since the distance between the beam bottom and the ground is small for the right span, most of the strain sensors were installed mainly in the middle cross-section of the left span to obtain the detailed strain variation. The subsequent analysis also focuses on the strain data in the left span. The wireless strain sensors and data acquisition system were utilized in the testing, which further simplifies the load testing, and the sensor layout is shown in Fig. 5.

After acquiring the strain, the strain response is filtered using the moving average to remove the noise. The data from strain sensor No. 4 in the bias load condition is shown in Fig. 6(a). The data in Fig. 6(a) is the response generated by the moving trolley traveling from right to left. Therefore, the peak appears on the right half of the picture because that is when the trolley is traveling exactly right above the sensor. There is a drift in the strain obtained from the measurement resulting in nonzeroing after the trolley moves off the bridge caused by the error of the sensor itself. Therefore, the strain data are dedrifted according to the a priori information that the strain should be zero before the

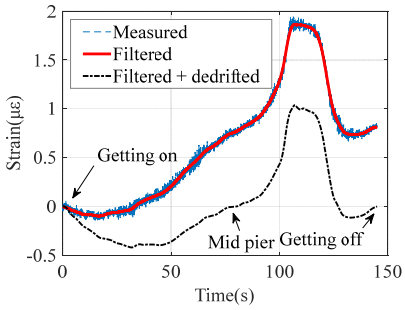

(a) Time-history strain

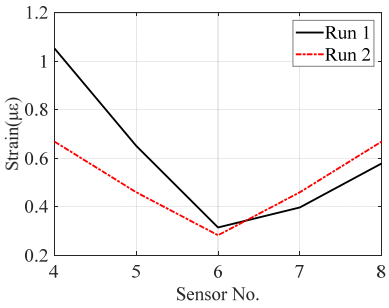

(b) Strain distribution of the bottom plate

Fig. 6 Strain data of the box girder

trolley gets on the bridge, after getting off the bridge and upon reaching the middle pier position. Based on the laboratory testing results of the sensor, a quadratic function is chosen to dedrift the strain data. In this paper, only the strain data on the bottom plate are used because the strain is larger and more reliable. Fig. 6(b) illustrates the strain distribution when the trolley moved to the middle of the left span during loading at Run1 and Run2, corresponding to the bias loading condition and the centerline loading condition, respectively.

5.1.2 Dynamic testing

The dynamic characteristics were extracted by measuring the acceleration response of the bridge under external load excitations. In order to ensure the accuracy of the modal parameters obtained and the convenience of the testing process, a force hammer was used to apply pulsed excitation to the bridge. A total of 54 acceleration sensors were arranged, as shown in Fig. 7(a). Each span of the bridge was divided into 10 equal parts, 9 sensors were arranged, and a total of 3 rows of sensors were arranged laterally. Three rows of acceleration sensors were installed at the midline and railings of the bridge. The field sensor installation is shown in Fig. 7(b). The frequencies and mode shapes are identified from the acceleration response using the stochastic subspace technique, and the first six orders of frequencies and vertical mode shapes are obtained, as shown in Fig. 8. The 1st, 2nd, 4th and 6th order mode shapes are bending modes, and the 3rd and 5th order mode shapes are torsional modes. These data will be applied to match the dynamic characteristics in model updating. It is worth mentioning that the inclination of the bridge deck was also considered when extracting mode shapes from finite element model for model updating.

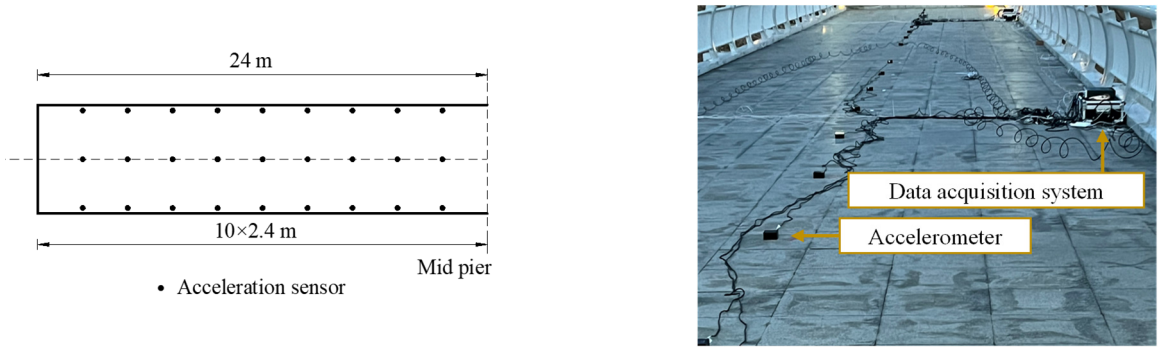

(a) Schematic (b) Photograph

Fig. 7 Acceleration sensor arrangement

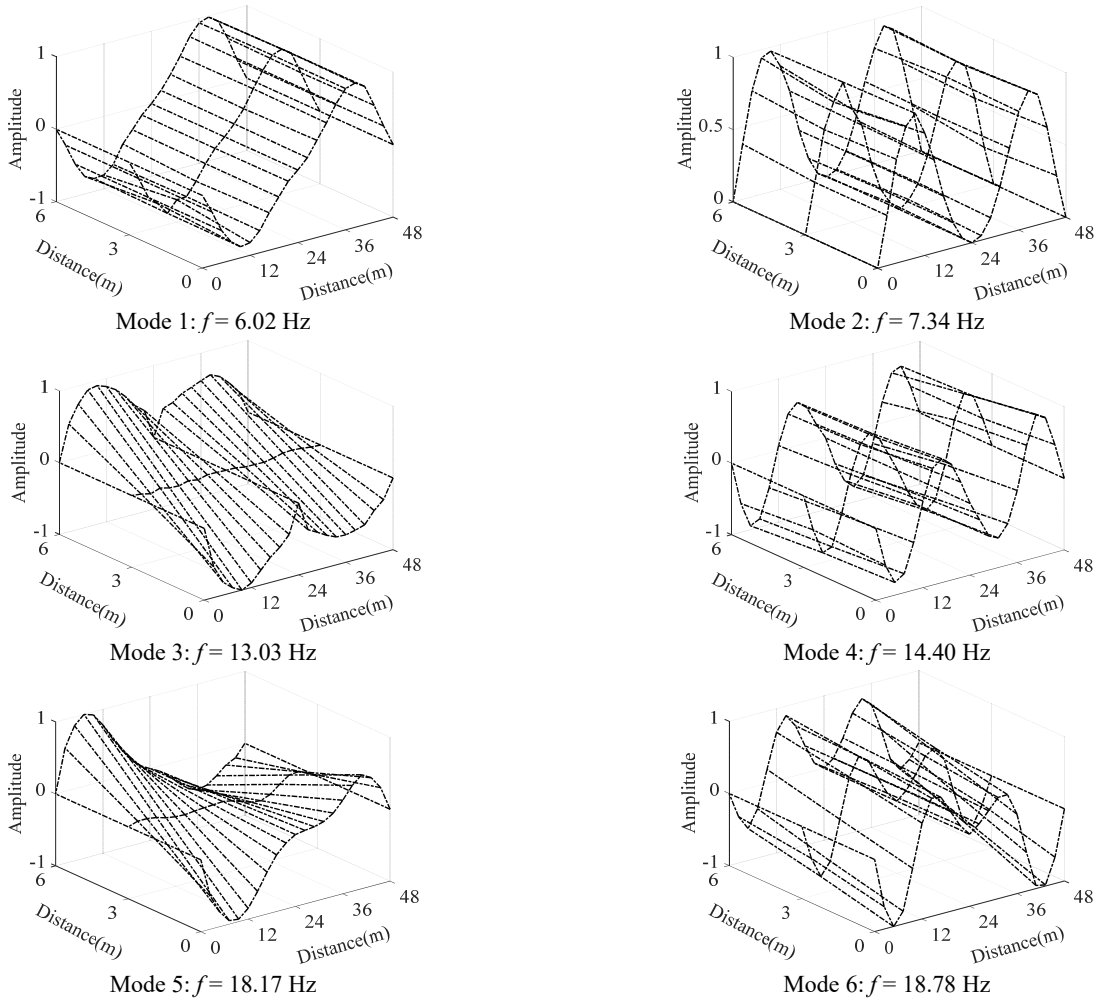

Fig. 8 Results of field-identified frequencies and mode shapes

5.1.3 Static load testing for verification

To verify the correctness of the optimization results, the bridge was loaded with water bags to obtain the displacement responses of the bridge in each span. Static load testing was conducted twice. The loading positions of water bags were the middle and quarter spans of the left span, respectively. The displacement sensors were installed at the mid-span of each span of the bridge and were used to measure the displacement induced by the water bags. Each side of the bottom plate of the mid-span section was installed with a displacement sensor. In total, four displacement meters were installed. Field installation of the displacement sensor is shown in Fig. 5(b). After the water bag was filled, the displacement meter was read to obtain the displacement data. Load-side displacement data were used because of the higher signal-to-noise ratio and reliability. There displacement data were used to verify the accuracy of the corrected model. The static loading cases

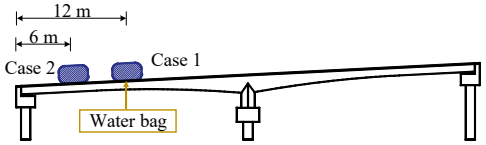

(a) Water bag loading schematic

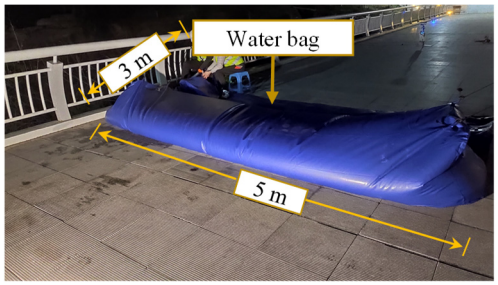

(b) Loading photograph of case 1

Fig. 9 Static load testing

and field loading photograph are shown in Fig. 9.

5.2 Model updating for load rating

5.2.1 Description of finite element model

The test bridge is a box girder bridge, and the finite element model is established by shell element based on Reissner-Mindlin plate theory (Liew and Han 1997). The actual sizes of the top plate, bottom plate and other members of the box girder bridge are simulated using shell element of the same thickness. The box girder bridge is modeled with an angle of inclination, which is consistent with reality. Bridge pavement is considered during modeling. The height of the box girder is varied along the longitudinal direction from 0.8 m to 1.8 m, which is also accurately simulated during modeling. For the boundary conditions, the two ends of the bridge are simulated as simply supported, and the bottom of the pier is completely fixed. The middle of the box girder is cemented to the pier. Spring elements are added to the two ends and pier positions in the finite element model to simulate a real bridge where the boundary conditions are not ideal simple support and fixed connection (Aloisio *et al*. 2020). The reason for adding spring elements at the pier locations is that there is a large amount of dirt on both sides of the piers, resulting in some additional constraints on the piers, which are not out of a completely free state (Meng *et al*. 2020). The finite element model of the test bridge is shown in Fig. 10.

5.2.2 Results of model updating

The optimization parameters need to be selected according to the sensitivity analysis before the model updating. In this field, optimization parameters are not only the common material parameters but also the additional stiffness of the support, as it is not an ideal boundary in real structures. The alternative parameters to be optimized are the concrete density, elastic modulus of the top plate, web, bottom plate, transverse diaphragm, pier, deck pavement, additional stiffness of translation and rotation of the left and

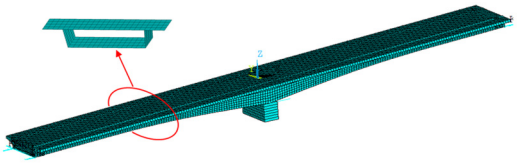

Fig. 10 Shell element model of box girder bridge

right supports and additional stiffness of translation and rotation of the pier. The sensitivity analysis is carried out according to Eqs. (9) and (10). Due to the different optimization ranges of the parameters and the impact on the final objective function, the sensitivity analysis is divided into two groups. The first group includes the density (ρ), elastic modulus of the top plate (E_{tp}), web (E_w), bottom plate (E_{bp}), transverse diaphragm (E_{td}) and pier (E_p), and bridge deck pavement (h_p). The second group is the additional translation and rotation stiffness at the left supports (K_{tl}, K_{rl}), right supports (K_{tr}, K_{rr}) and pier (K_{tp}, K_{rp}). The results of the sensitivity analysis are shown in Fig. 11. The difference in sensitivity of each parameter is obvious, and the optimization parameters that are sensitive to the objective function are selected for model updating. Finally, the parameters selected for model updating are ρ, E_{tp}, E_w, E_{bp}, K_{tl}, K_{rl}, K_{tr}, K_{rr}. The Rosenbrock algorithm is used for the model updating, and the range of optimization parameters is set according to engineering experience. The range of density is set as 80%~120% of the initial value, and the range of elastic modulus is 80~150% of the initial value. The additional translation and rotation stiffnesses are set to 0~10^{10} N/m and 0~10^{8} N · m/rad, respectively. In the optimization, the weight coefficients β and γ in Eq. (4) and Eq. (6) are set to 1. The weight coefficient λ_i in Eq. (7) is set according to Eq. (8). The optimization results and the corresponding objective results are shown in Tables 1-2.

Table 1 shows that the density of the bridge changes very little, while the elastic modulus increases in all cases, with a relatively larger increase in the top plate and web than the others. The significant increase in elastic modulus is due to the following two reasons: (a) The contribution of reinforcement and prestressing steel is not considered in the modeling; and (b) The configuration simplification of the bridge cross-section during modeling reduces the structural stiffness. Therefore, the elastic modulus will increase after model updating. The additional stiffness of the left and right supports had a significant contribution to the model updating results, which is consistent with the sensitivity analysis results. The contribution of the translational stiffness is greater than the contribution of the rotational stiffness. Table 2 shows that the values of the objective function decreased considerably after the model updating for frequency and strain, while the objective function of the mode shape was basically unchanged, which means that the measured results of the mode shape and finite element results were originally consistent.

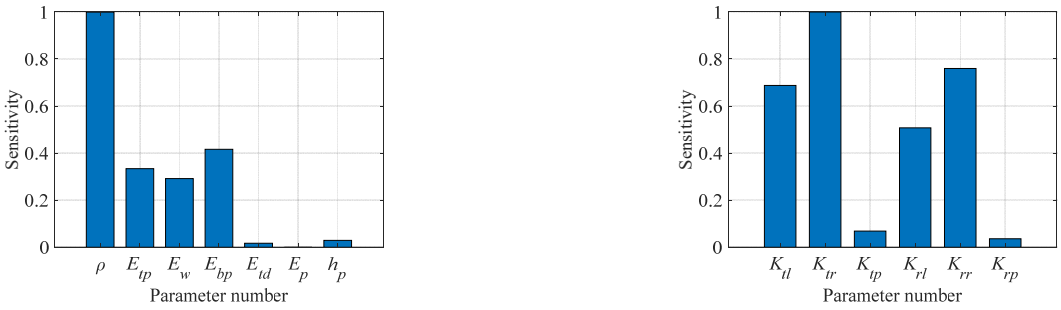

(a) Parameters of Group 1 (b) Parameters of Group 2

Fig. 11 Sensitivity analysis of parameters

Table 1 Parameter optimization results through model updating

Parameter number	Initial value	Lower boundary	Upper boundary	Updated value	Variation
ρ	2500 kg/m^3	2000 kg/m^3	3000 kg/m^3	2536 kg/m^3	1.2%
E_{tp}	3.45E10 Pa	2.76E10 Pa	5.18E10 Pa	5.18E10 Pa	50%
E_w	3.45E10 Pa	2.76E10 Pa	5.18E10 Pa	4.83E10 Pa	39%
E_{bp}	3.45E10 Pa	2.76E10 Pa	5.18E10 Pa	4.19E10 Pa	21%
K_{tl}	0 N/m	0 N/m	1E10 N/m	2.57E9 N/m	/
K_{tr}	0 N/m	0 N/m	1E10 N/m	1.68E9 N/m	/
K_{rl}	0 N·m/rad	0 N·m/rad	1E8 N·m/rad	1.45E7 N·m/rad	/
K_{rr}	0 N·m/rad	0 N·m/rad	1E8 N·m/rad	5.64E7 N·m/rad	/

Table 2 Variation of the objective function

	F_1	F_2	F_3	F
Before updating	1	1	1	3
After updating	0.0454	0.9660	0.0042	1.0158

5.2.3 Validation of updated model

The correctness of the optimization results is verified in terms of frequency, MAC, strain, and displacement. The static displacements are not used for model updating, so they can be used to verify the updated model. The frequency, MAC, and static displacement results are shown in Tables 3-4, and the strain results are shown in Fig. 12.

As Table 3 shows, there is good agreement between the updated model and the actual structure in terms of frequency and mode shape, with a maximum error of frequency of only 7%. Considerable improvement in the MAC results is not observed because the initial results of the model are in good agreement with the real structure. Fig. 12 shows that the strain distribution of the bottom plate is much improved, although not completely consistent with the measured distribution. Moreover, the error of the axial force is only 6% of the measured value. Finally, the displacements under static loads that were not used in the model updating were applied to verify the updated model. Table 4 shows that the maximum error is approximately 10% in the displacement between the updated model and the field measurement under the same load. Considering that the structural stiffness is large and the static load is relatively small, the measured displacement is vulnerable to

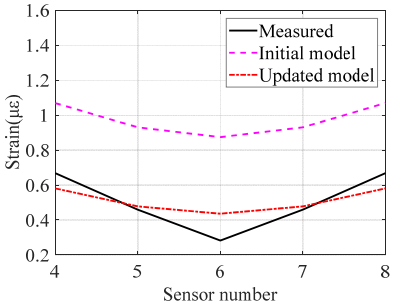

Fig. 12 Strain results of bottom plate

some measurement noise. Therefore, the error of the displacements can be acceptable. To date, this model has been updated successfully, and the model can be used for further evaluation of this bridge.

5.3 Results and discussion of load rating

The previous section has completed the model updating using testing data, and the updated model can represent the actual operational performance of the bridge. Therefore, the load capacity of the bridge can be evaluated directly through this model. The load effects of the bridge can be obtained by applying the corresponding loads (self-weight, pavement, and pedestrian load) on the updated model, and the rating factor can be calculated according to Eq. (14). When the rating factor is greater than 1, the bridge is considered to have sufficient resistance to live loads, and the load capacity of the bridge is determined to meet the

Table 3 Frequency and MAC results

Mode order	Frequency				MAC	
	Initial value (Hz)	Measured value (Hz)	Updated value (Hz)	Error	Initial value	Updated value
1	3.71	6.02	5.88	2.35%	0.974	0.996
2	5.97	7.34	7.65	4.31%	0.993	0.998
3	11.70	13.03	13.94	7.01%	0.938	0.939
4	12.30	14.40	14.41	0.11%	0.959	0.976
5	14.02	18.17	17.01	6.37%	0.858	0.867
6	15.28	18.78	18.07	3.70%	0.851	0.869

Table 4 Static load testing results for verification

Case	Load position	Load weight (t)	Measured deflection (mm)	Calculated deflection (mm)	Error
1	Mid span	6	0.316	0.337	6.64%
2	Quarter span	5.3	0.238	0.214	10.08%

requirements.

The rating factor is calculated for the bending capacity as an example, and the mid-span section of the left span is selected to be checked where the largest positive bending moment occurs. The unfavorable design live load is applied to calculate the max load effects through updated model. For a positive bending moment, the pedestrian load should be fully distributed on the left span. The load effects of self-weight, pavement, and pedestrian load are 1.66×10^6 N $\cdot$ m, 2.08×10^5 N $\cdot m$, and 1.04×10^6 N $\cdot m$, respectively. In addition, the bending resistance at this location needs to be calculated according to the code *AASHTO LRFD Bridge Design Specifications* (AASHTO 2020). The bending resistance is calculated as 1.07×10^7 N $\cdot m$. Considering that the bridge has been built recently and is in good condition without any apparent defects and cracks, the bending capacity of the bridge is not discounted. The coefficients γ_{DC}, γ_{DW}, and γ_{LL} in Eq. (14) are selected according to the design load and inventory evaluation rating in the *MBE*. The coefficients γ_{DC}, γ_{DW}, and γ_{LL} are set as 1.25, 1.50, and 1.75, respectively. The rating factor of 4.56 can be obtained according to Eq. (14).

From the result of the rating factor, it can be concluded that the bending capacity of the bridge at the checking section can meet the requirements of the design live load. According to the rating factor and Eq. (15), the safe load capacity of the bridge can be determined. When the specified design load is 5 kN/m^2, the modified safe load capacity limit can be considered as 22.8 kN/m^2. It can be concluded that this box girder bridge also has a sufficient load capacity reserve and that the design is conservative.

6. Conclusions

This paper introduces a method for load rating of box girder bridges based on rapid testing using moving loads. A static and dynamic testing process and a corresponding load rating method are proposed. This method is finally applied to evaluate the capacity of a box girder bridge. The following conclusions can be drawn.

- A rapid testing procedure for box girder bridges is proposed. The quasi-influence factors are obtained using moving loads across the bridge, and additional structural dynamic information about modal frequency and mode shapes is provided by the dynamic testing as a complement to the rapid static testing. The testing method can significantly reduce the number of sensors and the time of traffic interruption during the testing.
- A finite element modeling method for the box girder bridge is established. The static and dynamic behaviors can be represented by the model established by shell elements, and the model can be properly updated through the combined static and dynamic objective functions, which are established according to the rapid static and dynamic testing data. The updated model is in good agreement with the actual bridge in the dynamic and static characteristics of the bridge at the same time.
- A load rating method is proposed for box girder bridges based on the updated bridge model. The rating factors are calculated directly using the load effects of the updated model, and each bridge member can be evaluated separately based on the actual load effects instead of being modified by the same adjustment factor, which can avoid conservative or risky assessment results. A field application is further presented, and the proposed load rating method is verified to be rational and feasible for box girder bridges.

Acknowledgments

This research work was jointly supported by the National Natural Science Foundation of China (Grant Nos. 52078102, 52322807 and 51978128), the Fundamental

Research Funds for the Central Universities (Grant Nos. DUT21JC38 and DUT22ZD213), and the Key Laboratory of Performance Evolution and Control for Engineering Structures in Tongji University, Ministry of Education (Grant No. 2022KF-1).

References

AASHTO (2011), The Manual for Bridge Evaluation, AASHTO, Farmington Hills, MI, USA.

AASHTO (2020), AASHTO LRFD Bridge Design Specifications, AASHTO, Farmington Hills, MI, USA.

Abedin, M., y Basalo, F.J.D.C., Kiani, N., Mehrabi, A.B. and Nanni, A. (2022), "Bridge load testing and damage evaluation using model updating method", *Eng. Struct.*, **252**, 113648. https://doi.org/10.1016/j.engstruct.2021.113648

Aloisio, A., Alaggio, R. and Fragiacomo, M. (2020), "Dynamic identification and model updating of full-scale concrete box girders based on the experimental torsional response", *Constr. Build. Mater.*, **264**, 120146. https://doi.org/10.1016/j.conbuildmat.2020.120146

Altunişik, A.C., Kalkan, E., Okur, F.Y., Karahasan, O.Ş. and Ozgan, K. (2020), "Finite-element model updating and dynamic responses of reconstructed historical timber bridges using ambient vibration test results", *J. Perform. Constr. Facil.*, **34**(1), 04019085. https://doi.org/10.1061/(ASCE)CF.1943-5509.0001344

Brincker, R., Zhang, L.M. and Andersen, P. (2001), "Modal identification of output-only systems using frequency domain decomposition", *Smart Mater. Struct.*, **10**(3), 441-445. https://doi.org/10.1088/0964-1726/10/3/303

Chang, S.T. (2004), "Shear lag effect in simply supported prestressed concrete box girder", *J. Bridge Eng.*, **9**(2), 178-184. https://doi.org/10.1061/(ASCE)1084-0702(2004)9:2(178)

Hester, D., Koo, K., Xu, Y., Brownjohn, J. and Bocian, M. (2019), "Boundary condition focused finite element model updating for bridges", *Eng. Struct.*, **198**, 109514. https://doi.org/10.1016/j.engstruct.2019.109514

Jung, D.-S. and Kim, C.-Y. (2013), "Finite element model updating on small-scale bridge model using the hybrid genetic algorithm", *Struct. Infrastruct. Eng.*, **9**(5), 481-495. https://doi.org/10.1080/15732479.2011.564635

Liew, K.M. and Han, J.B. (1997), "Bending analysis of simply supported shear deformable skew plates", *J. Eng. Mech.*, **123**(3), 214-221. https://doi.org/10.1061/(ASCE)0733-9399(1997)123:3(214)

Lin, S.-W., Du, Y.-L., Yi, T.-H. and Yang, D.-H. (2022), "Model Updating Using Bridge Influence Lines Based on an Adaptive Metamodel Global Optimization Method", *J. Bridge Eng.*, **27**(3), 04022003. https://doi.org/10.1061/(ASCE)BE.1943-5592.0001839

Martini, A., Tronci, E.M., Feng, M.Q. and Leung, R.Y. (2022), "A computer vision-based method for bridge model updating using displacement influence lines", *Eng. Struct.*, **259**, 14. https://doi.org/10.1016/j.engstruct.2022.114129

Meng, K., Cui, C., Liang, Z., Li, H. and Pei, H., (2020), "A new approach for longitudinal vibration of a large-diameter floating pipe pile in visco-elastic soil considering the three-dimensional wave effects", *Comput. Geotech.*, **128**, 103840. https://doi.org/10.1016/j.compgeo.2020.103840

MOT (Ministry of Transport of the People's Republic of China), (2011), JTG/T-J21-2011 Specifications for Inspection and Evaluation of Loadbearing Capacity of Highway Bridges, China Communications Press, Beijing, China.

Ren, W.X. and Zong, Z.H. (2004), "Output-only modal parameter identification of civil engineering structures", *Struct. Eng. Mech., Int. J.*, **17**(3-4), 429-444. https://doi.org/10.12989/sem.2004.17.3_4.429

Sanayei, M., Phelps, J.E., Sipple, J.D., Bell, E.S. and Brenner, B.R. (2012), "Instrumentation, nondestructive testing, and finite-element model updating for bridge evaluation using strain measurements", *J. Bridge Eng.*, **17**(1), 130-138. https://doi.org/10.1061/(ASCE)BE.1943-5592.0000228

Schlune, H., Plos, M. and Gylltoft, K. (2009), "Improved bridge evaluation through finite element model updating using static and dynamic measurements", *Eng. Struct.*, **31**(7), 1477-1485. https://doi.org/10.1016/j.engstruct.2009.02.011

Sun, Z., Siringoringo, D.M. and Fujino, Y. (2021), "Load-carrying capacity evaluation of girder bridge using moving vehicle", *Eng. Struct.*, **229**, 12. https://doi.org/ 10.1016/j.engstruct.2020.111645

Timoshenko, S.P. and Young, D.H. (1968), *Theory of Structures*, McGraw-Hill. New York, NY, USA.

Xin, Y., Li, J., Wang, X. and Hampson, K. (2022), "Load-Carrying Capacity Assessment of an Existing Highway Bridge Based on Hybrid Finite-Element Model Updating", *J. Perform. Constr. Facil.*, **36**(3), 04022028. https://doi.org/10.1061/(ASCE)CF.1943-5509.0001729

Xue, M.-S., Yi, T.-H., Qu, C.-X. and Li, H.-N. (2022), "Deck Flexibility Identification of Bridges through a Submode Shape Combination Screening Method without a Reference Point", *J. Bridge Eng.*, **27**(8), 04022065. https://doi.org/ 10.1061/(ASCE)BE.1943-5592.0001908

Yang, D.H., Yi, T.H. and Li, H.N. (2017), "Coupled fatigue-corrosion failure analysis and performance assessment of RC bridge deck slabs", *J. Bridge Eng.*, **22**(10), 04017077. https://doi.org/10.1061/(ASCE)BE.1943-5592.0001108

Yang, D.H., Yi, T.H., Li, H.N. and Zhang, Y.F. (2018), "Correlation-based estimation method for cable-stayed bridge girder deflection variability under thermal action", *J. Perform. Constr. Facil.*, **32**(5), 04018070. https://doi.org/10.1061/(ASCE)CF.1943-5509.0001212

Yang, D.H., Zhou, H., Yi, T.H., Li, H.N. and Bai, H.F. (2022), "Joint deterioration detection based on field-identified lateral deflection influence lines for adjacent box girder bridges", *Struct. Control. Health Monit.*, **29**(10), e3053. https://doi.org/10.1002/stc.3053

Zhang, H., DesRoches, R., Yang, Z. and Liu, S. (2010), "Experimental and analytical studies on a streamlined steel box girder", *J. Constr. Steel Res.*, **66**(7), 906-914. https://doi.org/10.1016/j.jcsr.2010.02.001

Zheng, X., Yi, T.-H., Zhong, J.-W. and Yang, D.-H. (2022), "Rapid evaluation of load-carrying capacity of long-span bridges using limited testing vehicles", *J. Bridge Eng.*, **27**(4), 04022008. https://doi.org/10.1061/(ASCE)BE.1943-5592.0001838

Zordan, T., Briseghella, B. and Liu, T. (2014), "Finite element model updating of a tied-arch bridge using Douglas-Reid method and Rosenbrock optimization algorithm", *J. Traffic Transp. Eng.*, **1**(4), 280-292. https://doi.org/10.1016/S2095-7564(15)30273-7